



Photon + b jet production at CDF

The CDF Collaboration

(Dated: July 17, 2006)

Measurements of photon + b jet production, obtained with a dataset of 340 pb^{-1} , are presented. Cross-sections are measured for all events containing photons with transverse energy above 26 GeV, and differentially in bins of photon transverse energy between 26 and 70 GeV. Our results agree with leading order predictions of photon + b jet production.

I. INTRODUCTION

Events containing an isolated, high transverse energy (E_T) photon and an identified b jet are interesting to study for both QCD and new physics analyses. A measurement of the production cross-section of these events tests predictions of b jet production at the Tevatron. An excess in any photon + b channel could signal new physics, for example through light stop or techniomega production [1].

In this conference note we describe a measurement of the photon + b cross-section. We present the cross-section both as a function of photon E_T , in order to test QCD predictions at different energy scales, and for all photons with an E_T exceeding 26 GeV to gain maximal statistical sensitivity to deviations that could signal new physics production. We describe the data and Monte Carlo datasets used to carry out the analysis, and our event selection, in section II. The cross-section determination is described in section III and results are given in section IV. Section V outlines the sources of systematic error in the measurement. Finally, conclusions are drawn in section VI.

II. DATASETS AND EVENT SELECTION

A. Datasets

This analysis uses events triggered by an isolated, high energy ($> 25 \text{ GeV}$) photon trigger. A dataset corresponding to an integrated luminosity of $340 \pm 20 \text{ pb}^{-1}$ is used to perform the measurement. For reference, the CDF detector is described in detail in [2].

Pythia is used to simulate photon + jet production at leading order (LO). The minimal q^2 scale of the interaction is set to 15 GeV, CTEQ5L is used to model the parton density functions, and tune A is used for what concerns the

underlying event. An approximately equivalent luminosity of this Monte Carlo dataset is used to compare to data. Next to leading order comparisons have not yet been made.

B. Event selection

Candidate events must pass the isolated high energy photon trigger, contain an isolated central photon of E_T exceeding 26 GeV, and a jet of corrected energy exceeding 20 GeV within a pseudorapidity region of $|\eta| < 1.5$. The jet must also lie outside a cone of $dR = \sqrt{d\phi^2 + d\eta^2} = 0.7$ surrounding the photon candidate. We use displaced secondary vertices to identify heavy flavour jets. A positive tag is found when the secondary vertex is more than two standard deviations away from the beam position, and in the same direction away from the beam position as the jet momenta. We consider only those events having a positive tag in our cross-section calculation.

Photon candidates are obtained by placing requirements on: the ratio of hadronic to electromagnetic energy deposited; the agreement of the shower profile with that expected for an electromagnetic deposit; calorimetric and track energy in a cone around the photon candidate; adjacent calorimetric cluster energies to ensure isolation.

The jet, photon and b tag efficiencies (ϵ_j , ϵ_γ and ϵ_{tag} respectively), are determined from LO Monte Carlo and are typically 84 – 100%, 55%, and between 40 – 48% respectively in the photon E_T range considered in the analysis. The photon and b tag efficiency have been cross-checked against data; the photon selection efficiency agrees, and a scale factor is applied to the b tag efficiency to reflect observed differences [3]. Jet energy corrections (a major component of the jet efficiency) have been calculated using data. The trigger efficiency (ϵ_{trg}) is determined from data and ranges between 98.7% and 99.9%.

III. CROSS SECTION MEASUREMENT

The cross-section is defined as follows:

$$\sigma(\gamma + b; E_{T\gamma} > 26, |\eta_\gamma| < 1.1, E_{Tj} > 20, |\eta_j| < 1.5, dR > 0.7) = \frac{No.\gamma + b}{\epsilon_\gamma \epsilon_j \epsilon_{trg} \epsilon_{tag} \int \mathcal{L}}$$

where $E_{T\gamma}$ denotes the transverse energy of the photon, η_γ its pseudorapidity, and E_{Tj} and η_j denote the transverse energy and pseudorapidity of the jet respectively. The quantity dR has been defined in the previous section. The integrated luminosity is denoted by $\int \mathcal{L}$.

A. Event composition

Our selected event sample consists of a mixture of signal and background, as photons and π^0 s (produced directly, or via K_s or η decay) pass the photon selection criteria with similar efficiencies.

In order to determine the number of signal photon + b jet events ($No.\gamma + b$) we adopt the following procedure:

1. The composition of the selected event sample is estimated by fitting the invariant mass of the secondary vertex to Monte Carlo templates.
2. The signal fraction is estimated using preshower (CPR) detector information in data.
3. The background composition is estimated using a jet triggered data sample.
4. The background b component is normalised to the background fraction and subtracted from the overall number of b events, to give the number of signal photon + b jet events.

Each step is discussed in more detail below.

B. Event sample composition

We use the invariant mass of the tagged secondary vertex to discriminate between b, c and light quark jets. Figure 1 shows secondary vertex mass distributions for each type which have been obtained from Monte Carlo. We fit the secondary vertex mass distribution in data to these templates allowing the normalisations to float in the fit [4]. Uncertainties due to data and template statistics, and correlations between template shapes, are reflected in the fit fraction statistical errors.

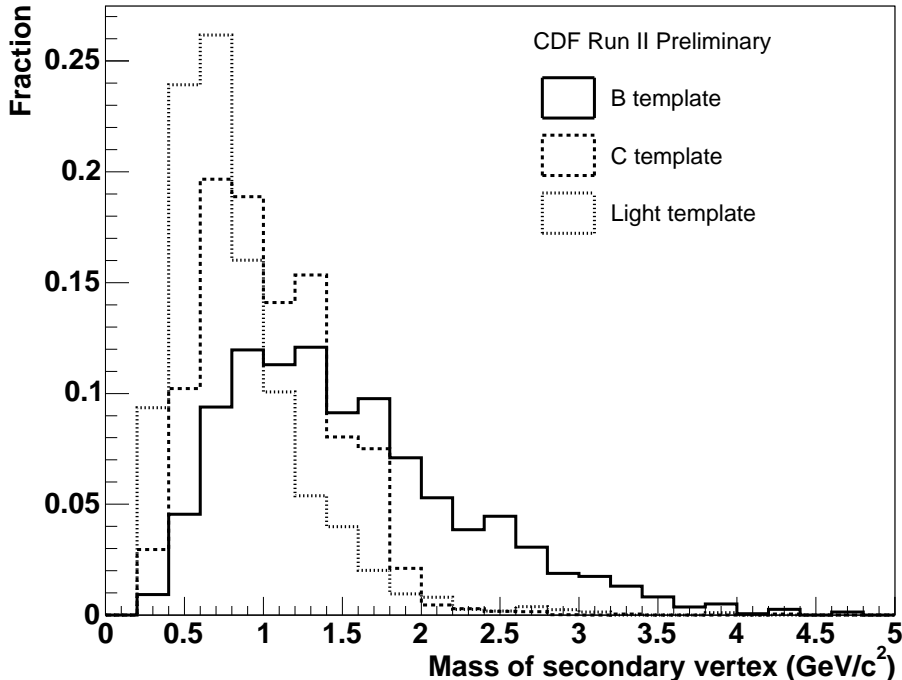


FIG. 1: Secondary vertex mass templates for b, c and light quark jets, obtained from Pythia Monte Carlo.

As the template shapes exhibit some dependence on tagged jet transverse energy we reweigh the mass distribution according to the jet E_T observed in data.

Figure 2 shows the fits to data in each bin of photon E_T . Figure 3 shows the fit for the full event sample which consists of the following fractions: 0.39 ± 0.02 of b; 0.39 ± 0.03 of c; 0.22 ± 0.03 of light jets.

C. Signal fraction determination

In order to estimate the number of photons in our sample, we use information from the CPR detector. Hits are detected in the CPR proportional chambers from photon conversions with a probability of approximately 60%. As backgrounds decay into two photons, these have twice the probability of leaving a hit and thus a detection probability of around 84%. This difference forms the basis for a statistical method which assigns each event a weight of being a photon, based on the photon candidate E_T , energy deposited and angle travelled through the CPR, and an estimate of detector material, pair production cross-sections and photon and background identification efficiency.

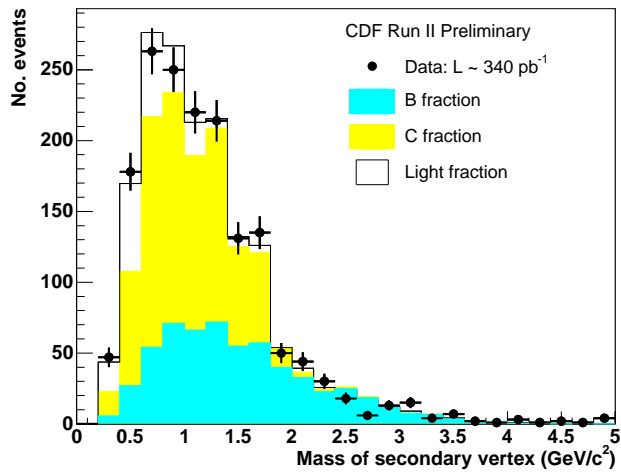
D. Background composition

Neutral pions form the main background to photons. We assume that the composition of tagged jets recoiling against a π^0 is identical to those recoiling against a π^\pm , and that this should not depend on the pions being isolated or having fragmented into jets, as long as the energy is known. We use data obtained using a jet trigger to estimate background composition. Events are selected by requiring one jet to pass the same minimum transverse energy and eta requirements as our signal, and which should also have a positive secondary vertex tag.

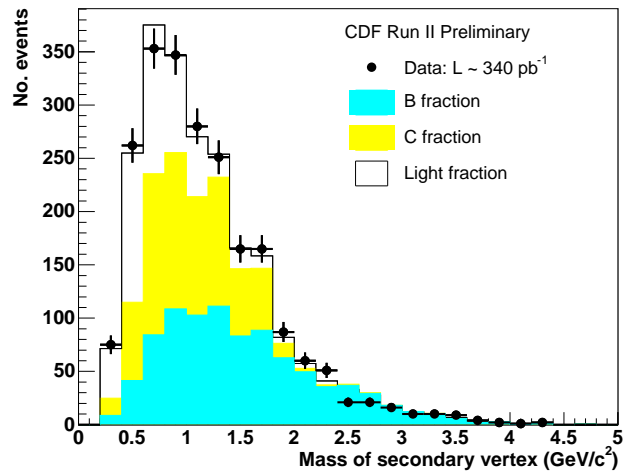
The background composition is estimated by fitting the secondary vertex mass spectrum to mass templates obtained with a corresponding jet Monte Carlo sample.

E. Signal photon + b jet event estimation

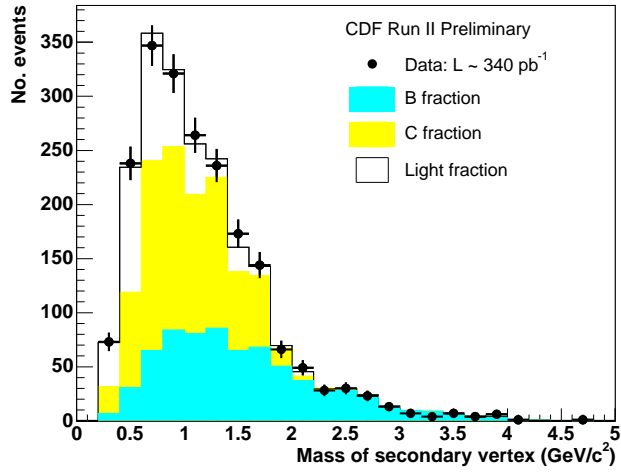
The background composition is normalised to the number of misidentified photons in data, and subtracted from the total number of b candidates to obtain the number of photon + b jet candidates. This will be divided by the efficiencies given earlier, and normalised by the integrated luminosity studied, to yield the cross-section.



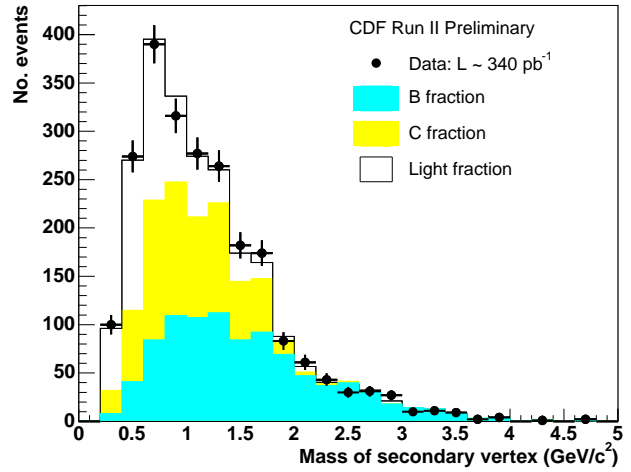
(a) Photon $E_T = 26 - 28$ GeV



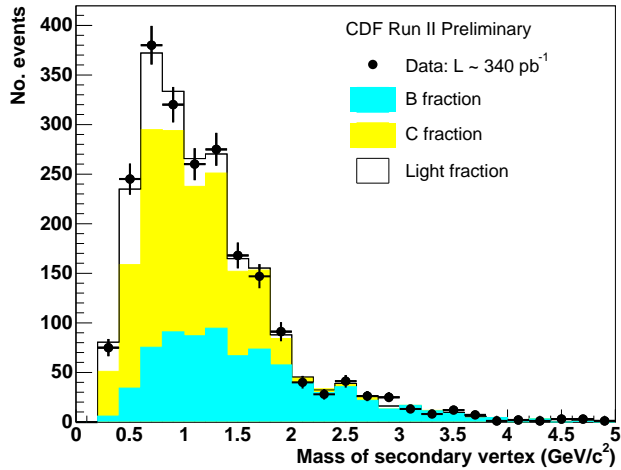
(b) Photon $E_T = 28 - 31$ GeV



(c) Photon $E_T = 31 - 35$ GeV



(d) Photon $E_T = 35 - 43$ GeV



(e) Photon $E_T = 43 - 70$ GeV

FIG. 2: Fits to secondary vertex mass distributions in the different photon E_T bins. The outcome of the fit is shown as a histogram, and the component estimated to be due to b (c) jets is overlaid in blue (yellow). Data are denoted by the points in each case.

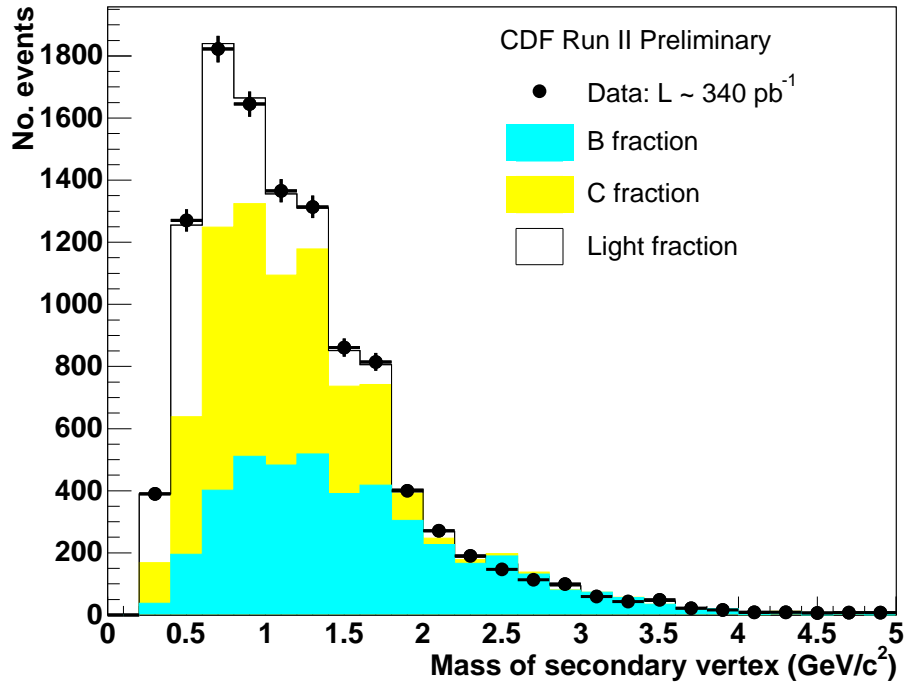


FIG. 3: Fits to secondary vertex mass distributions for the full event sample. The outcome of the fit is shown as a histogram, and the component estimated to be due to b (c) jets is overlaid in blue (yellow). Data are denoted by points.

IV. RESULTS

The inclusive cross-section for events containing a photon of $E_T > 26$ GeV is 42.0 ± 3.8 pb, where the error is statistical. The calculated differential photon + b jet cross-sections are given in table I in bins of photon E_T between 26 and 70 GeV. A full breakdown of the individual statistical error sources and their values is given in table II.

Photon E_T /GeV	26-28	28-31	31-35	35-43	43-70
$\sigma(\gamma + b)$ pb/GeV	2.93 ± 0.48	3.09 ± 0.44	1.46 ± 0.23	1.23 ± 0.17	0.23 ± 0.03

TABLE I: Differential photon + b jet cross-sections, as determined in each bin of photon E_T . All errors are statistical.

Photon E_T /GeV	26-28	28-31	31-35	35-43	43-70	> 26
Fake photon	± 0.32	± 0.28	± 0.15	± 0.10	± 0.02	± 1.7
B purity	± 0.27	± 0.25	± 0.13	± 0.09	± 0.02	± 2.3
B background	± 0.07	± 0.08	± 0.04	± 0.03	± 0.01	± 1.1
Photon efficiency	± 0.02	± 0.02	± 0.01	± 0.01	± 0.01	± 0.3
b jet efficiency	± 0.17	± 0.16	± 0.08	± 0.06	± 0.01	± 1.0
b tag efficiency	± 0.15	± 0.15	± 0.07	± 0.06	± 0.01	± 2.1
Total stat. error (pb/GeV)	± 0.48	± 0.44	± 0.23	± 0.17	± 0.03	± 3.8 pb

TABLE II: Sources of statistical error for photon + b jet production. Results are given for the differential and total cross-section measurements. Errors for the differential cross-section are given in units of pb/GeV, whereas those for the inclusive cross-section are in pb.

Sources of systematic error include: luminosity; fake photon estimate (ie. background fraction); jet efficiency; photon efficiency; template shapes (ie. b purity); background composition; b tagging efficiency. Each source is briefly described in the subsections below. The systematic errors are summarised in table III.

A. Luminosity

The luminosity measurement is subject to a $\pm 6\%$ uncertainty [5].

B. Fake photon estimate

Systematic uncertainties in the fake photon estimate arise from assumed values for: the CPR hit rate; the rate of backscattered showers; the fractional composition of fake photon backgrounds. These errors are summed in quadrature to yield the total systematic error due to this source.

C. Jet efficiency

Systematic uncertainties in the jet efficiency arise from two sources: uncertainties on the jet energy scale; the E_T dependance of the efficiency.

The systematic error associated to the jet efficiency scale is taken as the difference to nominal acceptance in Monte Carlo when the jet energy corrections are changed by $\pm 1\sigma$ [6]. The E_T dependance is dealt with separately in subsection V H.

D. Photon efficiency

Two sources of systematic error in the photon efficiency have been considered: imperfect Monte Carlo modelling of the efficiency and the effect of multiple $p\bar{p}$ interactions that may affect isolation criteria.

Studies of selection efficiency in $Z^0 \rightarrow e^+e^-$ events show that data and Monte Carlo are consistent. We have used the error of the comparison (1.2%) as a systematic error in this analysis. We have studied the selection efficiency as a function of the number of primary vertices observed in data and take the largest difference found (0.2%) as a systematic error.

Both errors are summed in quadrature to yield a total systematic error on photon efficiency.

E. Template shapes

The sample composition is determined by fitting templates of secondary vertex mass shapes to data distributions. If these templates are incorrect then the composition will be wrong. We have considered the following sources of systematic error on the template shapes: template shapes from jets containing one or two heavy quarks having different shapes; incorrect modelling of track inefficiency; fragmentation.

We find template shapes obtained from tagged jets containing one and two b quarks respectively are consistent, but those obtained from c and $c\bar{c}$ jets are not. We repeated composition fits (to both data and background simultaneously) using normal b and light templates and (a) a charm template made solely from single quark jets, and (b) two charm templates corresponding to single and double quark jets. The full difference in fractions obtained using these and the nominal fits is taken as a systematic error.

The systematic effect of unmodelled tracking inefficiency is larger. We remake templates imposing a 3% inefficiency on each track. The full difference in fractions obtained from fits using these and the nominal templates is taken as a systematic error. We apply the inefficiency to templates for both the signal and background sample fits simultaneously.

We assume that systematic effects of fragmentation modelling in Pythia are small, as template shapes made from Pythia and Herwig Monte Carlo are consistent, and do not assign an error to this source.

All template systematics are summed in quadrature to yield a total systematic error.

F. Background composition

Sources of systematic error on the background composition arise from: template shapes for one and two quark jets; the effect of track inefficiency; the assumption that jet triggered data is a valid background model. The first two errors have been considered in the previous section.

We have compared compositions obtained from datasets triggered by jet triggers at two different transverse energy thresholds and found them consistent. We have also checked that the composition is similar for tagged jets which are not the most energetic in the event, to test for trigger bias. We have used jet Monte Carlo to investigate whether the composition depends on the jet originating from a quark or gluon. We found that the compositions are consistent within statistical errors (approximately 2%) and took this as a systematic error.

G. B tagging efficiency

Systematic errors on the b tagging efficiency arise from: the scale factor used to multiply Monte Carlo predictions; the E_T dependence of the tagging; any difference in the tagging efficiency of jets containing one and two b quarks.

The error due to the scale factor is taken from [3] and is about 7%. The second error is dealt with in subsection V H. We determine tagging efficiency separately for jets containing one and two b quarks. The full difference between results obtained using each in turn is taken as a systematic error. All sources of systematic error are summed in quadrature to yield a systematic error.

H. Jet E_T modelling

We observe that the tagged jet transverse energy distribution is some 10% higher in data than photon + jet Monte Carlo. Mismodelled jet E_T affects jet efficiency, background composition and tagging efficiency.

We perform the analysis assuming that both signal and background produce jets of E_T matching that observed in data. The full difference in results obtained using this assumption, and the central value (where we assume the Monte Carlo value is correct for signal) is taken as a systematic error.

I. Total systematic error

All sources of systematic error considered in the measurement are given in table III.

Photon E_T /GeV	26-28	28-31	31-35	35-43	43-70	> 26
Luminosity	± 0.18	± 0.19	± 0.09	± 0.07	± 0.01	± 2.5
Fake photon estimate	+0.18 -0.20	+0.15 -0.17	+0.09 -0.13	+0.05 -0.07	+0.01 -0.02	+1.8 -2.7
Jet energy scale	+0.14 -0.15	+0.11 -0.06	+0.02 -0.04	± 0.02	± 0.01	± 1.0
Photon efficiency	± 0.04	± 0.05	± 0.02	± 0.02	± 0.01	± 0.6
Template shapes	+0.89 -0.39	+0.51 -0.36	+0.25 -0.20	+0.20 -0.14	+0.07 -0.03	+7.4 -4.0
Background composition	± 0.04	± 0.03	± 0.03	± 0.01	± 0.01	± 0.4
b tagging efficiency	+0.45 -0.18	+0.43 -0.19	+0.16 -0.09	+0.11 -0.07	+0.02 -0.01	+3.4 -2.6
Jet E_T modelling	-0.50	-0.35	-0.18	-0.13	-0.01	-3.5
Total sys. error (pb/GeV)	+1.04 -0.73	+0.72 -0.60	± 0.33	+0.26 -0.23	+0.08 -0.04	+8.8 -7.0 pb

TABLE III: Summary of systematic errors for the photon + b differential and total cross-sections. Errors for the differential cross-section are given in units of pb /GeV, whereas those for the inclusive cross-section are in pb.

VI. CONCLUSIONS

We have measured the photon + b jet production cross-section using 340 pb^{-1} of data taken by the CDF experiment. The cross-section is determined for all events with photon E_T exceeding 26 GeV, and differentially in five photon E_T

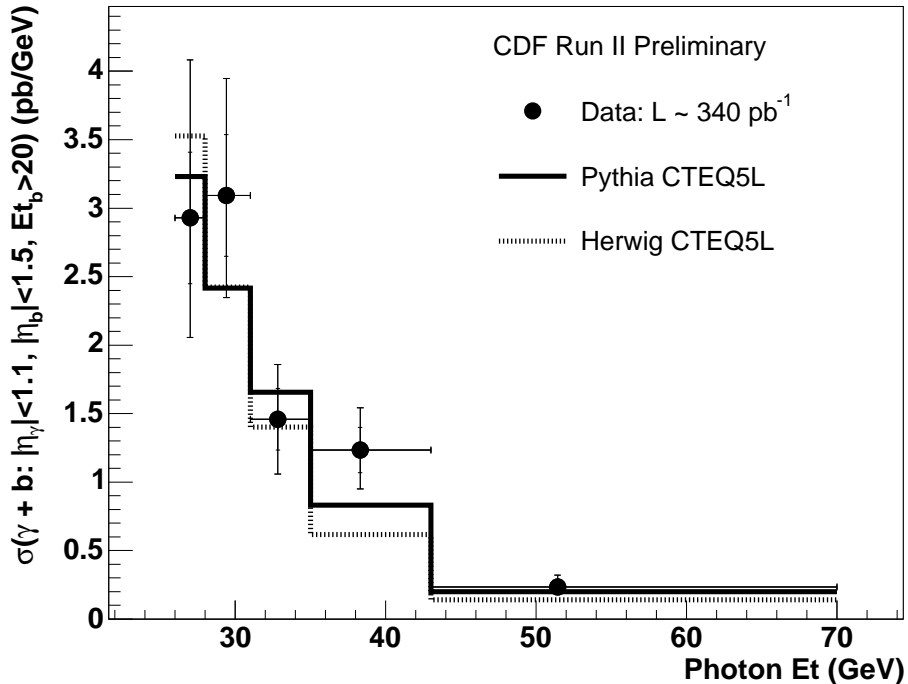


FIG. 4: Differential cross-section for photon + b production, shown as a function of photon transverse energy. Data are denoted by points, and the full and dotted lines show Pythia and Herwig predictions respectively. Statistical, and statistical summed in quadrature with systematic errors are shown.

Photon E_T /GeV	$\sigma(\gamma + b: \eta_\gamma < 1.1, \eta_b < 1.5, E_{Tb} > 20)$
26-28	$2.93 \pm 0.48^{+1.04}_{-0.73}$ pb/GeV
28-31	$3.09 \pm 0.44^{+0.72}_{-0.60}$ pb/GeV
31-35	$1.46 \pm 0.23 \pm 0.33$ pb/GeV
35-43	$1.23 \pm 0.17^{+0.26}_{-0.23}$ pb/GeV
43-70	$0.23 \pm 0.03^{+0.08}_{-0.04}$ pb/GeV
> 26	$42.0 \pm 3.8^{+8.8}_{-7.0}$ pb

TABLE IV: Differential and total cross-sections for photon + b jet production, listed as a function of photon E_T . The first error quoted is statistical, the second systematic. Note that the differential cross-section is given as the total cross-section in a photon E_T bin, divided by the bin width.

bins between 26 and 70 GeV. Our results are reported in table IV. They are consistent with leading order predictions by Pythia and Herwig, as shown in figure 4.

Acknowledgments

We thank the Fermilab staff and the technical staffs of the participating institutions for their vital contributions. This work was supported by the U.S. Department of Energy and National Science Foundation; the Italian Istituto Nazionale di Fisica Nucleare; the Ministry of Education, Culture, Sports, Science and Technology of Japan; the Natural Sciences and Engineering Research Council of Canada; the National Science Council of the Republic of China; the Swiss National Science Foundation; the A.P. Sloan Foundation; the Bundesministerium für Bildung und Forschung, Germany; the Korean Science and Engineering Foundation and the Korean Research Foundation; the Particle Physics and Astronomy Research Council and the Royal Society, UK; the Russian Foundation for Basic Research; the Comisión Interministerial de Ciencia y Tecnología, Spain; the European Community's Human Potential

- [1] T. Affolder *et. al.* *Phys. Rev.* **D 65**, 052006 (2002).
- [2] D. Acosta *et. al.* *Phys. Rev.* **D71** 032001 (2005).
- [3] See <http://www-cdf.fnal.gov/physics/new/top/public/btag/>
- [4] R. Barlow and C. Beeston, *Comp. Phys. Comm.* **77** (1993) 219-228.
- [5] S. Klimenko, J. Konigsberg, T. M. Liss, *FERMILAB-FN-0741* (2003)
- [6] See <http://www-cdf.fnal.gov/physics/new/top/public/jets/cdfpublic.html>